Effect of Adsorption Mechanism on Conduction in Single-molecule Pyrrole-based Sensor for AFB1

Fabrizio Mo, Yuri Ardesi, Chiara Elfi Spano, Massimo Ruo Roch, Gianluca Piccinini and Mariagrazia Graziano.

Corresponding author: fabrizio.mo@polito.it

Supplementary Information

SI 1. Theoretical Considerations And Analysis Tools

In this section, we deeply discuss some theoretical aspects of the work. Also, we introduce the analysis tools we use in the main text of the article. Interested readers find all the details in the cited references.

Recovery Time

The sensor recovery time is related to the time interval in which the AFB1-sensor interaction occurs. When the AFB1 is adsorbed onto the Au-8PyDT, the current begins being modulated and the SMS detects the AFB1 presence. The current modulation persists for all the time the AFB1 is adsorbed, and it stops, with a current coming to its original value, when the AFB1 is desorbed. Therefore, the desorption process determines the sensor recovery time.

To estimate the recovery time of the sensor, we rely on the well-established Harmonic Transition State Theory (HTST) [1]. The HTST approximation is good whenever the reaction barrier energy, in our case of the order of the adsorption energy, is very large compared to the thermal energy. In our work, in all the considered cases (namely, AC1, AC2, AC3, AC4) E_{ads} exceeds the 100 kJ/mol in absolute value, therefore being much greater than kt (k is the Boltzmann's constant and t the temperature), that at room temperature (300 K) is $kt = 2.5$ kJ/mol. According to HTST, the desorption reaction rate is [1]:

$$r_{des} = \frac{\Pi_i^{3N} \nu_i^R}{\Pi_i^{3N-1} \nu_i^S} \; exp\left(-\frac{E_{rb}}{kt}\right)$$

where N is the number of atoms, ν_i^R and ν_i^S are the normal mode frequencies at the reactant point (R) and at the reaction barrier saddle point (S), E_{rb} is the reaction energy barrier. The pre-exponential term corresponds to the ratio of the product of the vibrational modes before the reaction (at the reactant), over the product of the stable vibrational modes at the reaction saddle. In this standpoint, it represents an attempt frequency of reaction (i.e. desorption). Whereas, the exponential term is the Boltzmann probability that a vibration attempt along the reaction direction will overcome the barrier and produce the desorption of AFB1 from the sensor. The expression of r_{des} is functionally the same as the empirical Arrhenius' rate law. By defining $\nu = \frac{\Pi_i^{3N} \nu_i^R}{\Pi_i^{3N-1} \nu_i^S}$, and considering that in our case (desorption process) the reaction barrier is of the order of the adsorption energy $E_{rb} \approx |E_{ads}|$, one gets:

$$r_{des} \approx \nu \; exp\left(-\frac{|E_{ads}|}{kt}\right)$$

The sensor recovery time is thus:

$$\tau = \frac{1}{r_{des}} \approx \nu^{-1} \; exp\left(\frac{|E_{ads}|}{kt}\right)$$

that corresponds to equation (3) of the main text of the article.

To precisely calculate ν, and therefore r_{des} and τ, we should calculate the system dynamical matrix, and consider many system images on the reaction path (usually through a nudged elastic band calculation). Since such calculations are extremely computationally heavy, considering also the large number of atoms present in our system, and since we are interested in a first-order estimation of τ, we approximate ν starting from the AFB1 vibrational modes, that are known from literature

[2, 3, 4]. Indeed, our results demonstrate that no chemical bond is present between AFB1 and 8PyDT, and therefore we expect that vibrational attempts in the desorption reaction direction are caused by AFB1 vibrations or by its composing functional group vibrations (the electronic state of AFB1 and 8PyDT are only weakly modified when adsorption occurs). Therefore, we consider ν in the range $10^{12} \div 10^{14}$ Hz, which corresponds to AFB1 and its functional group vibrations [2, 3, 4], with a larger margin toward lower frequencies to account from eventual vibrational damping due to AFB1-8PyDT electrostatic interaction. With a range of ν, we are able to estimate a range of τ within what we expect the actual sensor τ belongs to. Moreover, we can estimate the temperature t at which the AFB1 desorption is significantly enhanced to ensure the sensor recovery in reasonable time intervals.

Analysis Tools

We make use of the following analysis tools:

- Mulliken population (MP) [5, 6, 7, 8]: It corresponds to the number of electrons that on average are close to a specific atomic site. We consider the valence electron shells, since they are the only perturbed electron shells in our case. If MP equals the element electron number the atom is neutral, if greater/lesser the atom is negatively/positively charged. We report the MP in terms of atomic charge normalized to the elementary charge q. The MP of orbital i is defined as:

$$MP_i = \sum_j D_{ij} S_{ij}$$

  where D is the density matrix and S the overlap matrix.

  It is possible to calculate the MP of an atom α as:

$$MP_\alpha = \sum_{i \in \alpha} \sum_j D_{ij} S_{ij}$$

- Electron Density (ED) [9, 10, 11]: We consider the electron density $n(\vec{r})$, as defined in the Hartree potential, through the solution of Poisson equation:

$$\nabla^2 V_H[n](\vec{r}) = -\frac{q^2}{4\pi\epsilon_0} n(\vec{r})$$

  with ϵ_0 vacuum permittivity and V_H Hartree potential.

- Electron Density Difference (EDD): The EDD $\delta n(\vec{r})$ is defined through the relation [11, 12]:

$$\delta n(\vec{r}) = n(\vec{r}) - \sum_i^{N_a} n_i(\vec{r})$$

  where N_a is the number of atoms in the system. The EDD highlights the regions of space in which there is an extra electron density w.r.t. isolated atoms. In other words, EDD is helpful in visualizing chemical bonds among atoms. Indeed, if the EDD is non-null among adjacent atoms, it indicates a presence of electrons, i.e. a chemical bond, among them.

- Electron Localization Function (ELF) [13]: ELF is a measure of the electron delocalization in space. It is 3D function [11] with values between 0 (free electron) and 1 (localized electron).

- Transmission Eigenstates (TEs) [14, 11]: TEs, together with the transmission coefficients (eigenvalues) are the solution of the eigenvalue problem for the transmission operator. In other words, TEs are the eigenstates of the quantum mechanical transmission matrix TM for the considered device. In general, TM is function of the electron energy E and momentum $\vec{k}$: $TM(E, \vec{k})$. In practice, TEs are useful to understand where the S-to-D transmission occurs in space.

  Relation between TEs and TS: Once the applied voltage V_{DS} is fixed, the transmission spectrum TS is only dependent on the electron energy E: $T(E, V_{DS}|_{fixed}) = T(E)$. For each electron energy E, the $T(E)$ value is given by the sum of all the transmission eigenvalues contributing to the total S-to-D transmittivity at that energy E. Each transmission eigenvalue is associated with a single TE. Therefore, for each electron energy E, there are more transmission coefficients (eigenvalues) contributing to $T(E)$, each one associated to one transmission channel, that in turn corresponds to a given TE.

- Transmission Pathways (TPs) [15, 11]: It is possible to split the transmission coefficient into local bond contributions, which can be both positive or negative (transmitted / backscattered electrons along the bond). Such local bond contributions can be represented by arrows with corresponding directions. The direction of the arrows thus corresponds also to the electron direction. We use TPs to understand where and how electron transmission occurs in space.

Voltage Dependent Sensor Response

The sensing mechanism relies on TS modifications produced by the AFB1 - Au-8PyDT interaction inside the BW energy range. The situation is depicted in Fig SI1(a). There are three possible cases: (i) The presence of AFB1 modifies the TS in the BW. In this case, the obtained ΔI_{DS} is large - Fig. SI1(b). (ii) The presence of the target modifies TS at E distant from the BW. In this case, the produced ΔI_{DS} is small or negligible - Fig.SI1(c). (iii) The presence of the target modifies the TS in the BW, but variations compensate each other. In this case, since I_{DS} is given by the integral of $T(E, V_{DS})$ in dE, the obtained ΔI_{DS} is small or negligible - Fig. SI1(d). The sensor response depends on V_{DS}, since, by varying V_{DS}, significant variations of TS can be included in the BW, resulting in significant current modulation - refer to equation (4) of the main text of the article. Further details can be found in [16, 17].

Figure SI1: (a) BW and Fermi function weighting effect on $T(E, V_{DS})$; (b), (c), (d) Examples of different target effects: green and black curves are referred to the cases in which the target is present and absent, respectively.

SI 2. Adsorption Energy

Table SI2: Calculated E_{ads} values in our previous works [16, 18]. Rotations in Z are fixed to 0°.

geometry	E_{ads} (kJ/mol)	geometry	E_{ads} (kJ/mol)
Y=0°, X=−25°	+158.65	Y=45°, X=−25°	-61.64
Y=0°, X=0°	+158.07	Y=45°, X=0°	-57.57
Y=0°, X=+25°	+166.18	Y=45°, X=+25°	-55.81
Y=0°, X=+45°	+152.81	Y=45°, X=+45°	-58.68
Y=90°, X=−25°	-74.28	Y=135°, X=−25°	-50.85
Y=90°, X=0°	+156.84	Y=135°, X=0°	-49.96
Y=90°, X=+25°	-56.48	Y=135°, X=+25°	-59.93
Y=90°, X=+45°	-67.66	Y=135°, X=+45°	-60.61
Y=180°, X=−25°	-53.32	Y=225°, X=−25°	-72.24
Y=180°, X=0°	-56.02	Y=225°, X=0°	-82.07
Y=180°, X=+25°	-57.65	Y=225°, X=+25°	-76.57
Y=180°, X=+45°	-63.07	Y=225°, X=+45°	-78.54
Y=270°, X=−25°	-91.06	Y=315°, X=−25°	-83.99
Y=270°, X=0°	-41.70	Y=315°, X=0°	-54.41
Y=270°, X=+25°	-45.09	Y=315°, X=+25°	-59.47
Y=270°, X=+45°	-53.19	Y=315°, X=+45°	-52.94

SI 3. AFB1 - Sensor Interaction Analysis
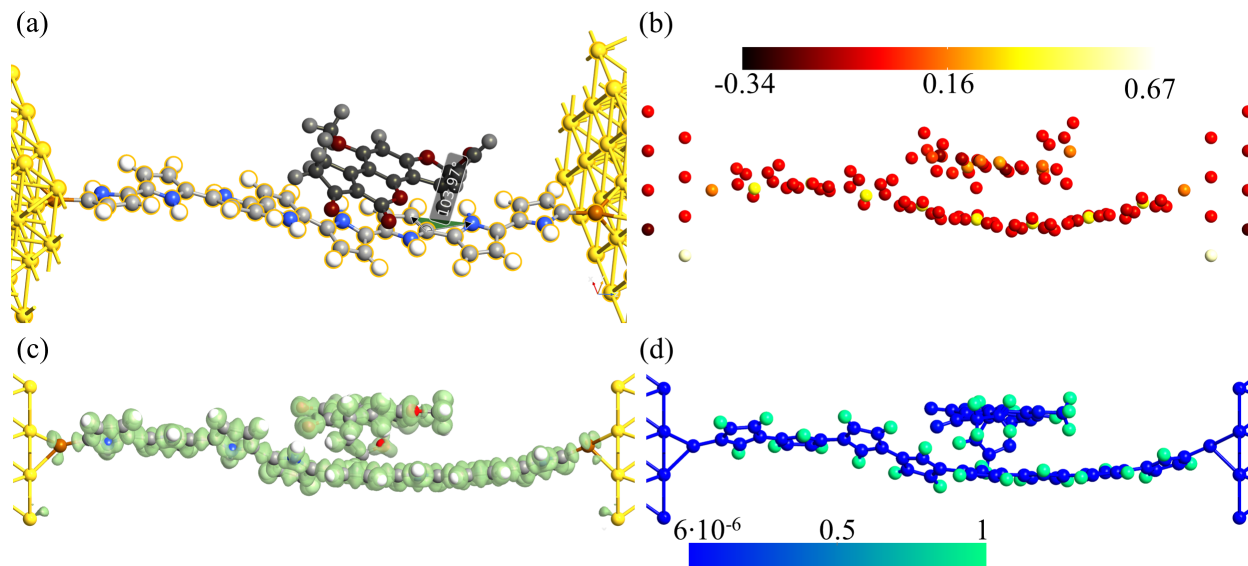
(a)

(b)

(c)

(d)

Figure SI3: (a) AC2 geometry -important differences with the isolated Au-8PyDT are reported and the Au-8PyDT detection element is highlighted for clarity; (b) Mulliken atomic charge, the color legend is intended in elementary charge; (c) electron density difference; (d) ELF, 1 indicates localized states and 0 completely delocalized ones.
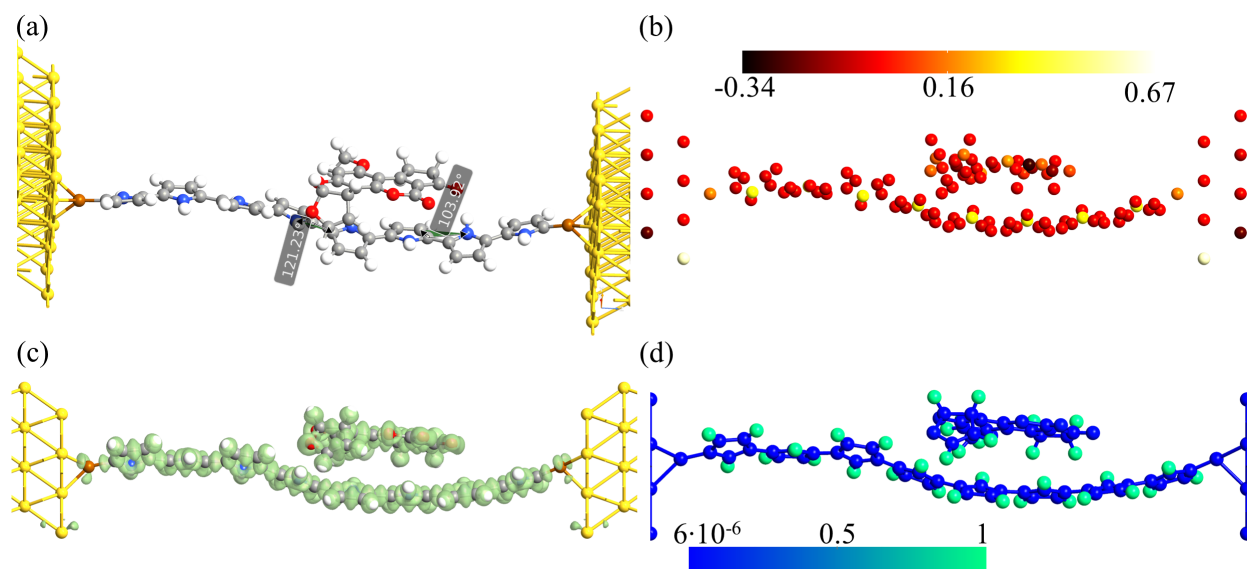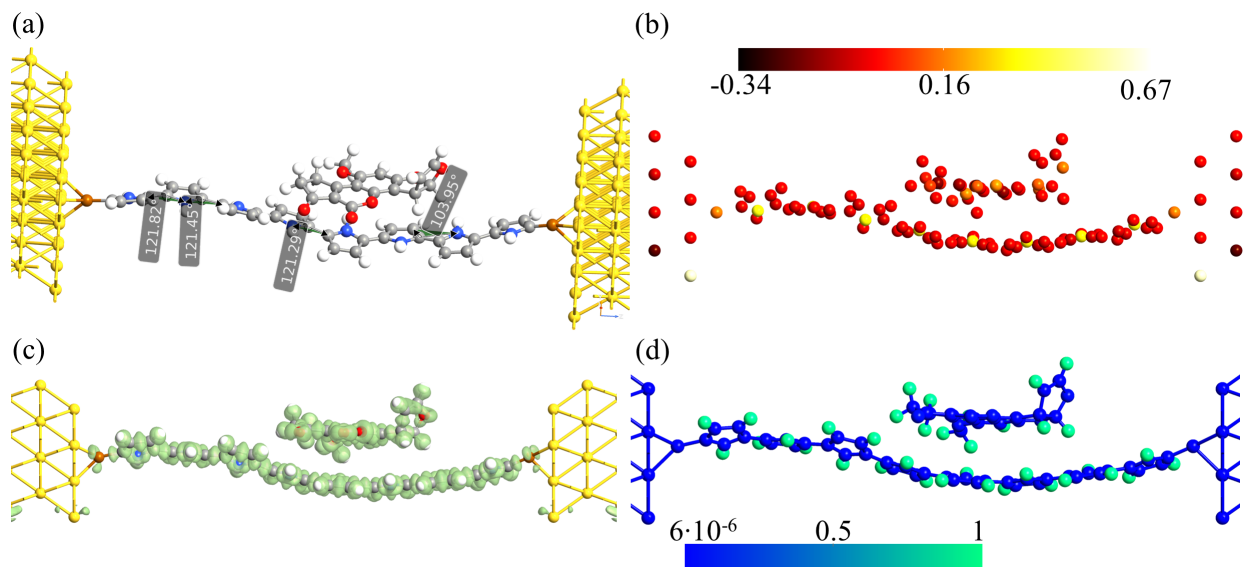
(a)

(b)

(c)

(d)

Figure SI4: (a) AC3 geometry -important differences with the isolated Au-8PyDT are reported; (b) Mulliken atomic charge, the color legend is intended in elementary charge; (c) electron density difference; (d) ELF, 1 indicates localized states and 0 completely delocalized ones.

Figure SI5: (a) AC4 geometry -important differences with the isolated Au-8PyDT are reported; (b) Mulliken atomic charge, the color legend is intended in elementary charge; (c) electron density difference; (d) ELF, 1 indicates localized states and 0 completely delocalized ones.

SI 5. Energetics Of The AFB1 - Sensor Interaction

Table SI6: Energy components of the AFB1-sensor interactions in the four most stable adsorption configurations: AC1, AC2, AC3, AC4. E_{TOT} is the total energy; E_{EL} is the electrostatic component; E_{XC} is the exchange-correlation component of the Kohn-Sham Hamiltonian; E_{vdW-D3} is the DFT-D3 (by Grimme and co-workers) correction for the van der Waals interactions; E_{KIN} is the kinetic contribution. All energies are in eV.

Configuration	E_{TOT}	E_{EL}	E_{XC}	E_{vdW-D3}	E_{KIN}
AC1	-174004.32651	-236192.23114	-47664.13592	-129.24278	109981.00491
AC2	-174003.72774	-236190.22169	-47663.71277	-129.19230	109979.12238
AC3	-174003.87743	-236189.66588	-236189.66588	-129.24271	109977.62433
AC4	-174003.74317	-236191.02225	-47663.98392	-129.19819	109980.18315

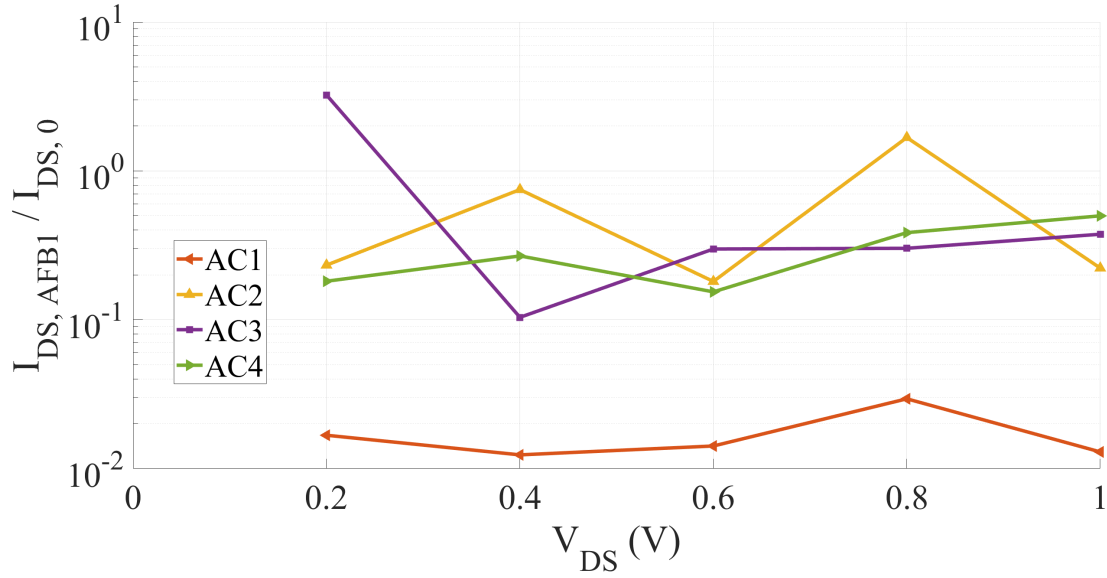# SI 6. Sensor Response And Electronic Transport Analysis

Figure SI7: $I_{DS,AFB1}/I_{DS,0}$ for the considered voltage values and adsorption configurations. At 0.2 V AC3 leads to too high ratio. At 0.4 V and 0.8 V AC2 leads to too high ratio. At 1 V a good situation is present even if the best one is for 0.6 V. Therefore, the optimum working point is at 0.6 V since all the ratios are minimized.
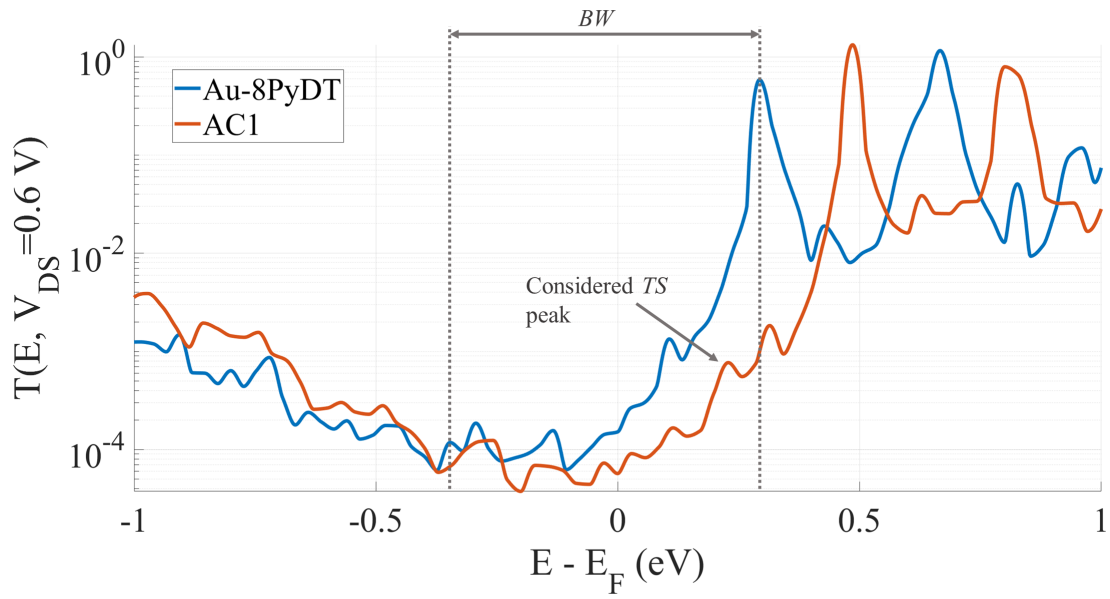
Figure SI8: AC1 $T(E)$ at fixed V_{DS}=0.6 V. The AC1 TS peak for which the TE and TPs are calculated is indicated with the arrow.
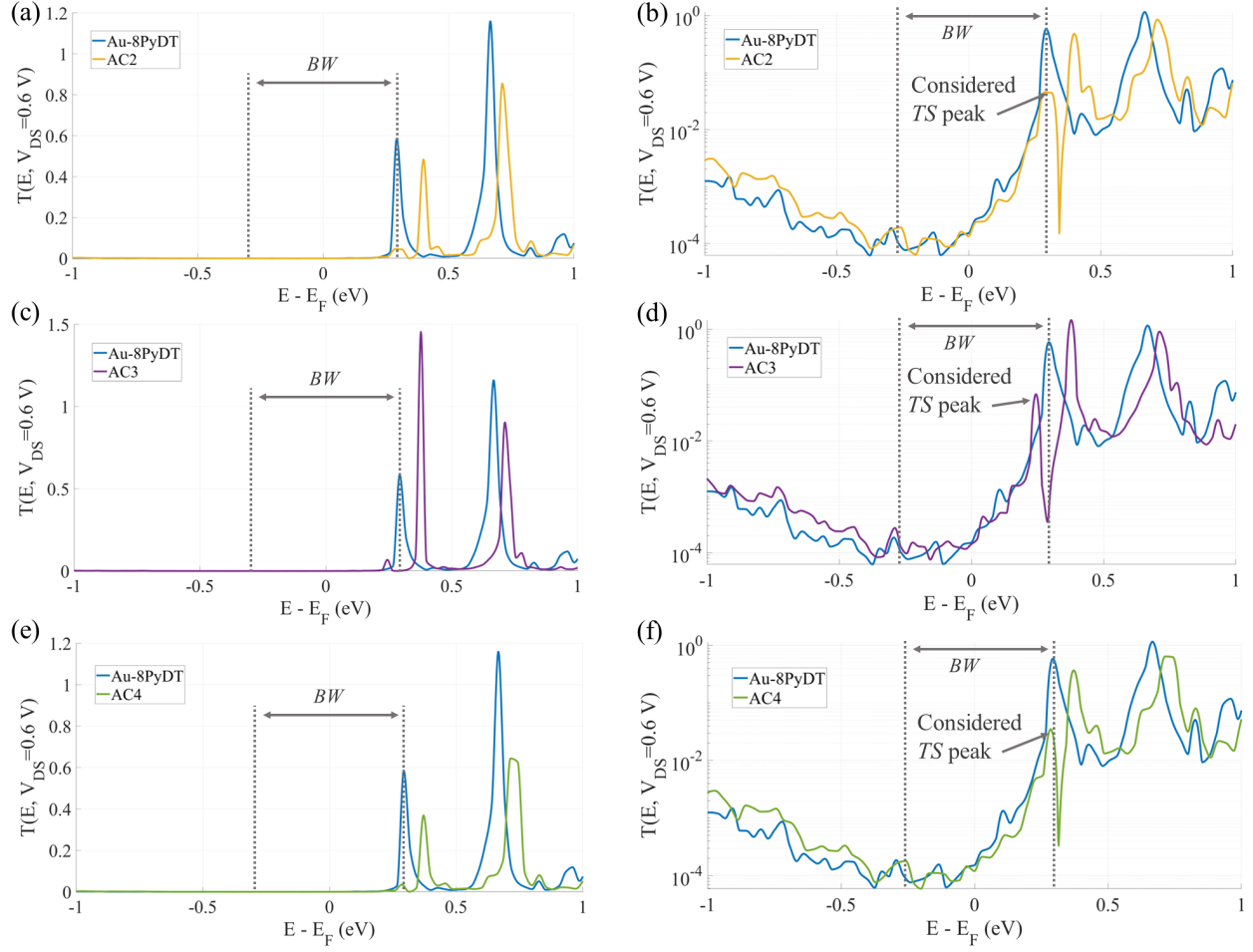
Figure SI9: AC2 $T(E)$ at fixed V_{DS}=0.6 V: (a) linear scale, (b) logarithmic scale; AC3 $T(E)$ at fixed V_{DS}=0.6 V: (c) linear scale, (d) logarithmic scale; AC4 $T(E)$ at fixed V_{DS}=0.6 V: (e) linear scale, (f) logarithmic scale. The TS peaks for which the TE and TPs are calculated are indicated with the arrows.
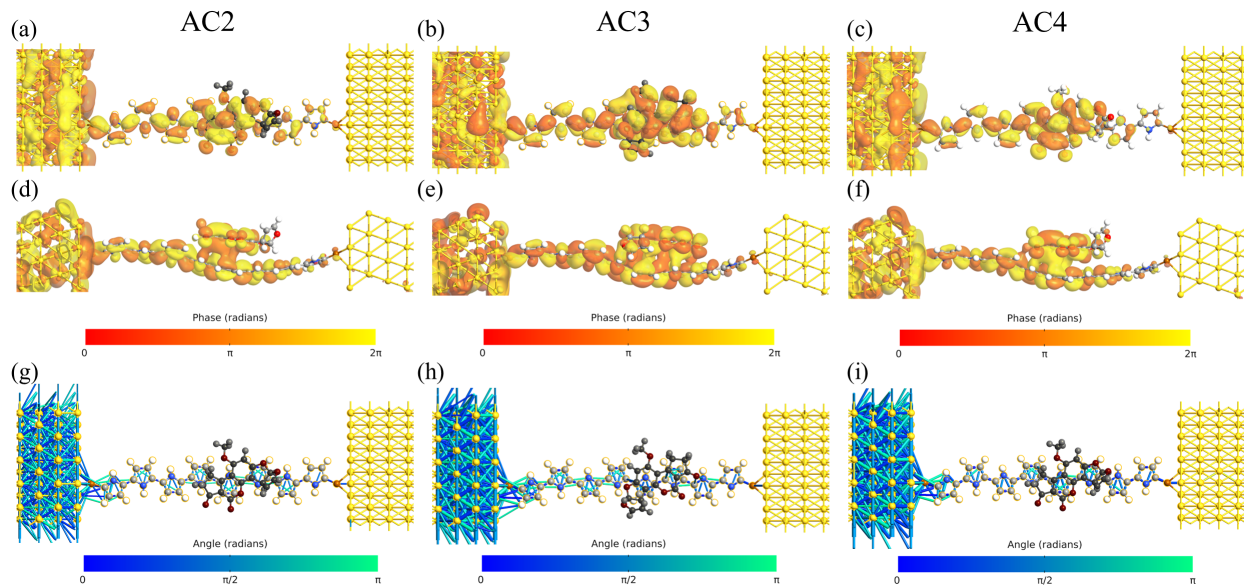
Figure SI10: Main TEs within the considered BW (V_{DS}=0.6 V), top views: (a) AC2, (b) AC3, (c) AC4; side views: (d) AC2, (e) AC3, (f) AC4. TPs for (g) AC2, (h) AC3, (i) AC4.

References

[1] G. H. Vineyard, "Frequency factors and isotope effects in solid state rate processes," *Journal of Physics and Chemistry of Solids*, vol. 3, no. 1, pp. 121–127, 1957. [Online]. Available: https://www.sciencedirect.com/science/article/pii/0022369757900598

[2] F. Billes, Ágnes M. Móricz, E. Tyihák, and H. Mikosch, "Simulated vibrational spectra of aflatoxins and their demethylated products and the estimation of the energies of the demethylation reactions," *Spectrochimica Acta Part A: Molecular and Biomolecular Spectroscopy*, vol. 64, no. 3, pp. 600–622, 2006. [Online]. Available: https://www.sciencedirect.com/science/article/pii/S1386142505004294

[3] K.-M. Lee, J. Davis, T. J. Herrman, S. C. Murray, and Y. Deng, "An empirical evaluation of three vibrational spectroscopic methods for detection of aflatoxins in maize," *Food Chemistry*, vol. 173, pp. 629–639, 2015. [Online]. Available: https://www.sciencedirect.com/science/article/pii/S0308814614016628

[4] J. A. Agwupuye, P. A. Neji, H. Louis, J. O. Odey, T. O. Unimuke, E. A. Bisiong, E. A. Eno, P. M. Utsu, and T. N. Ntui, "Investigation on electronic structure, vibrational spectra, nbo analysis, and molecular docking studies of aflatoxins and selected emerging mycotoxins against wild-type androgen receptor," *Heliyon*, vol. 7, no. 7, p. e07544, 2021. [Online]. Available: https://www.sciencedirect.com/science/article/pii/S2405844021016479

[5] R. S. Mulliken, "Electronic population analysis on lcao–mo molecular wave functions. i," *The Journal of Chemical Physics*, vol. 23, no. 10, pp. 1833–1840, 1955. [Online]. Available: https://doi.org/10.1063/1.1740588

[6] ——, "Electronic population analysis on lcao–mo molecular wave functions. ii. overlap populations, bond orders, and covalent bond energies," *The Journal of Chemical Physics*, vol. 23, no. 10, pp. 1841–1846, 1955. [Online]. Available: https://doi.org/10.1063/1.1740589

[7] ——, "Electronic population analysis on lcao-mo molecular wave functions. iii. effects of hybridization on overlap and gross ao populations," *The Journal of Chemical Physics*, vol. 23, no. 12, pp. 2338–2342, 1955. [Online]. Available: https://doi.org/10.1063/1.1741876

[8] ——, "Electronic population analysis on lcao-mo molecular wave functions. iv. bonding and antibonding in lcao and valence-bond theories," *The Journal of Chemical Physics*, vol. 23, no. 12, pp. 2343–2346, 1955. [Online]. Available: https://doi.org/10.1063/1.1741877

[9] P. Atkins and R. Friedman, *Molecular Quantum Mechanics*. OUP Oxford, 2011. [Online]. Available: https://books.google.it/books?id=9k-cAQAAQBAJ

[10] F. Jensen, *Introduction to computational chemistry*, 2nd ed. John Wiley & sons, 2007.

[11] S. Smidstrup, T. Markussen, P. Vancraeyveld, J. Wellendorff, J. Schneider, T. Gunst, B. Verstichel, D. Stradi, U. Martinez, A. Blom, M. Brandbyge, and K. Stokbro, "QuantumATK: an integrated platform of electronic and atomic-scale modelling tools," *Journal of Physics: Condensed Matter*, vol. 32, no. 1, p. 015901, oct 2019.

[12] J. M. Soler, E. Artacho, J. D. Gale, A. García, J. Junquera, P. Ordejón, and D. Sánchez-Portal, "The siesta method for ab initio order-n materials simulation," *Journal of Physics: Condensed Matter*, vol. 14, no. 11, p. 2745, mar 2002. [Online]. Available: https://dx.doi.org/10.1088/0953-8984/14/11/302

[13] A. D. Becke and K. E. Edgecombe, "A simple measure of electron localization in atomic and molecular systems," *The Journal of Chemical Physics*, vol. 92, no. 9, pp. 5397–5403, 1990. [Online]. Available: https://doi.org/10.1063/1.458517

[14] S. Datta, *Electronic transport in mesoscopic systems*. Cambridge University Press, 1995.

[15] G. C. Solomon, C. Herrmann, T. Hansen, V. Mujica, and M. A. Ratner, "Exploring local currents in molecular junctions," *Nature Chemistry*, vol. 2, no. 3, pp. 223–228, Mar 2010. [Online]. Available: https://doi.org/10.1038/nchem.546

[16] F. Mo, C. E. Spano, Y. Ardesi, M. R. Roch, G. Piccinini, and M. Graziano, "Single-molecule aflatoxin b1 sensing via pyrrole-based molecular quantum dot," in *2022 IEEE 22nd International Conference on Nanotechnology (NANO)*, 2022, pp. 153–156.

[17] F. Mo, Y. Ardesi, M. R. Roch, M. Graziano, and G. Piccinini, "Investigation of amperometric sensing mechanism in gold–c60–gold molecular dot," *IEEE Sensors Journal*, vol. 22, no. 20, pp. 19 152–19 161, 2022.

[18] F. Mo, C. E. Spano, Y. Ardesi, M. Ruo Roch, G. Piccinini, and M. Graziano, "Design of pyrrole-based gate-controlled molecular junctions optimized for single-molecule aflatoxin b1 detection," *Sensors*, vol. 23, no. 3, 2023. [Online]. Available: https://www.mdpi.com/1424-8220/23/3/1687